

PCCP

Accepted Manuscript



This is an *Accepted Manuscript*, which has been through the Royal Society of Chemistry peer review process and has been accepted for publication.

Accepted Manuscripts are published online shortly after acceptance, before technical editing, formatting and proof reading. Using this free service, authors can make their results available to the community, in citable form, before we publish the edited article. We will replace this *Accepted Manuscript* with the edited and formatted *Advance Article* as soon as it is available.

You can find more information about *Accepted Manuscripts* in the [Information for Authors](#).

Please note that technical editing may introduce minor changes to the text and/or graphics, which may alter content. The journal's standard [Terms & Conditions](#) and the [Ethical guidelines](#) still apply. In no event shall the Royal Society of Chemistry be held responsible for any errors or omissions in this *Accepted Manuscript* or any consequences arising from the use of any information it contains.

Cite this: DOI: 10.1039/c0xx00000x

www.rsc.org/xxxxxx

ARTICLE TYPE

Electrokinetic desalination using honeycomb carbon nanotubes (HC-CNT): a conceptive study by molecular simulation

Qile Chen, Xian Kong, Jipeng Li, Diannan Lu*, Zheng Liu*

Received (in XXX, XXX) Xth XXXXXXXXX 20XX, Accepted Xth XXXXXXXXX 20XX

DOI: 10.1039/b000000x

A new concept of electrokinetic desalination using a CNT honeycomb was presented through molecular dynamics simulation. The preferential translocation of ions towards the outlets near two electrodes were realized by applying an electric field perpendicularly to bulk fluid flow in CNT network, which, in the meantime, generated deionized water flux discharged from the central outlets. The effects of the major factors such as electric field strength, numbers of separation units, diameter of CNT, and ion concentration on the desalination were examined, respectively. It was shown that over 95% salt rejection and around 50% fresh water recovery were achieved by present module by applying an electric field of 0.8 V/nm. CNT diameter, which is critical to ion rejection without the electric field, had marginal effect on the desalination of this new module when a strong electric field was applied. The desalination was not sensitive to ion concentration, indicating that its excellent workability for a wide range of water salinity, e.g., from brackish water to seawater. PMF profile revealed a free energy barrier as large as 2.0-6.0 kcal/mol for ions to move opposite to the implemented electrical force. Above-mentioned simulation confirmed the high potential of CNT honeycomb in water desalination.

Introduction

The lack of clean and fresh water threatens billions of people worldwide and takes over millions of lives every year¹. To address these problems, great efforts have been constantly devoted to novel reverse-osmosis (RO) membrane that enables a high and exclusive water transport. It was firstly shown by Hummer *et al.*² using molecular dynamics simulation that the water flux inside carbon nanotube (CNT) could be as much as three to four orders of magnitude of that expected from macroscopic hydrodynamics. Later Granick *et al.*³ and Falk *et al.*⁴ simulated effects of the hydrophobicity of nanotube walls and the smooth energy landscape on the water flux. Corry *et al.* showed that CNT of 0.9 nm in diameter could give a nearly 100% salt rejection.⁵ The fouling-resistant property of CNT, being attributed to its hydrophobic surface and narrow inner pore⁶, is also advantageous for being used as membrane materials⁷. All these have raised great interest in exploring the application of CNT in water desalination⁸⁻¹².

The molecular dynamics simulation of water desalination using aligned CNTs showed that once the diameter of CNT is below 0.9 nm, ions are rejected due to high-energy penalty for the dehydration. Once the diameter of CNT is above 0.9 nm, however, salt rejection will no longer be satisfactory^{5, 13}. Above simulations were validated by experiments using 3-nm-diameter membranes¹⁴. Sub-nanometer CNT synthesis is available using laser ablation^{15, 16}, but only single water chain can be passing through the tube, causing relatively low water conductance. An alternate way to enhance the CNT membrane performance is to

modify the CNTs so that the electrostatic interaction and steric hindrance are employed simultaneously for ion rejection^{9, 17-19}. However and unfortunately, as simulated by Corry *et al.*⁹ and observed by Fornasiero *et al.*²⁰ the enhanced ion rejection by CNT surface modification is obtained at a compromise of water flux, due to counter-ion occlusion at the entrance of the CNT. More recently, Chan *et al.*²¹ simulated a zwitterions modified CNT composite membrane and obtained a high ion rejection and a high water flux.

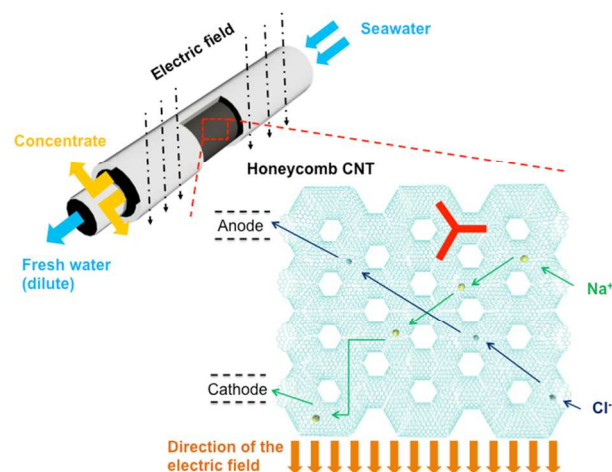


Fig.1 Schematic illustration of the honeycomb CNT (HC-CNT) device

Cite this: DOI: 10.1039/c0xx00000x

www.rsc.org/xxxxxx

ARTICLE TYPE

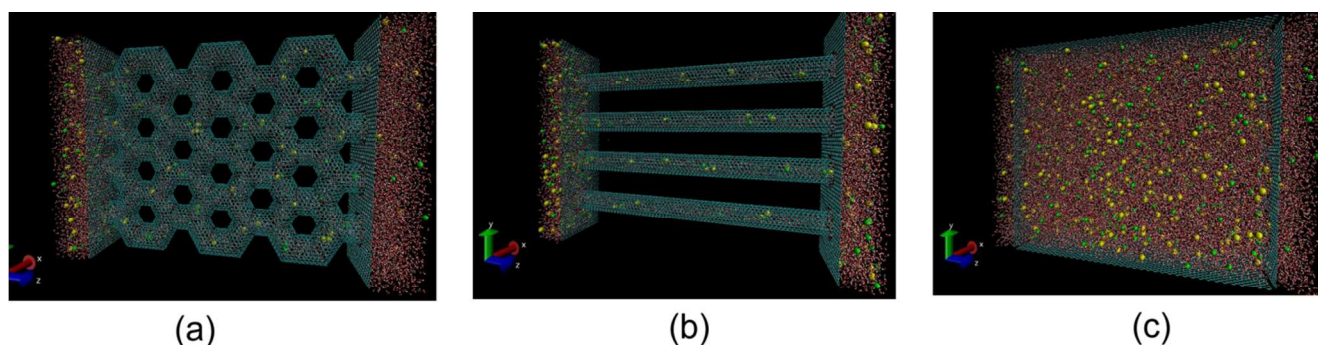


Fig.2 Nanodevice model for desalination: (a) HC-CNT membrane model; (b) A-CNT membrane model; (c) B-CNT membrane model

Electric field has been applied for water desalination processes such as electrodialysis (ED) and capacitive deionization (CDI). CDI utilizes also an electric field being vertical to the bulky water matrix but fails to handle high salinity seawater due to limited electrode capacities²². Introduction of an alternating electric field parallel to the flow direction in CNT or a point charge near CNT surface is effective to enhance the transport flux of pure water, but low efficiency for separation of water and ions²³⁻²⁶.

Here we present a novel and conceptive CNT device, *i.e.*, honeycomb-CNT (HC-CNT) for electrokinetic desalination. It is composed of multiple Y-junction units, where one of the units is colored in red, as shown in Figure 1. A vertical electric field is applied to the bulky water flux and thus drives the ions towards the electrode area, noted as anode and cathode in the Figure 1, and simultaneously reduces the ionic concentration of the water flux from the middle outlet. The concentrated ions are discharged from the outlets in the electrode area and thus prevent the concentration polarization. The continuous mode, by nature, is advantageous for industrial practice.

To demonstrate this idea, here we present a molecular dynamics (MD) simulation of the desalination process using this HC-CNT. We firstly simulated the ion and water transport in the CNT network in the presence of electric field. Then the factors that affect the ion rejection and water flux were examined, respectively. The issues that underpinned the energy consumption and the process efficiency were discussed, as well as the availabilities of HC-CNT devices or equipments.

Model and Simulation Methods

Models

HC-CNT membrane model: CNTs with (10,10), (12,12) and (14,14) armchair structures and flat graphenes were generated using Carbon Nanostructure Builder Plugin²⁷. CNTs are all 1.5 nm in length before being assembled into the honeycomb-shaped structures. The connectivity between channels is achieved by the assembled Y-shaped CNTs. The bulky fluid is driven by the hydrostatic pressure along +z axis. The electric field is applied at y-axis and drives the migration of Na⁺ (yellow) and Cl⁻ (green) ions, resulting in concentrated ion streams at the outlets near the

cathode and anode, and meanwhile, the dilute stream from the middle outlets. Here we define one separation unit as a 56 Å-long hexagon-shaped CNTs, thus the model shown in Figure 2 (a) has 3 separation units. Each separation unit is hexagon-shaped, containing two Y-junctions with a unit length around 56 Å. Graphene layers which are positioned at $z = \pm 82$ Å, together with the assembled Y-shaped CNTs within two layers consist of the CNT membrane.

Aligned-CNT (A-CNT) membrane model: An aligned-CNT (A-CNT) membrane model shown in Figure 2 (b) was constructed as reference [9]. The structural and operational parameters are the same as HC-CNT, including all the parameters of CNT and flat graphene, membrane thickness, pore density, hydrostatic pressure difference and ion concentration. The major difference is that the aligned CNT membrane has no vertical connectivity brought by the Y-shaped CNTs.

Bulky-CNT (B-CNT) membrane model: To illustrate the desalination mode of CDI process, bulky-CNT (B-CNT) model was constructed and indicated in Figure 2 (c). In this model, the membrane areas are no longer filled by CNTs. Instead, two flat graphenes are placed at top and bottom of simulation box, which represent capacitance. The thickness of the membrane and the overall ion concentration are essentially the same with the two previous designs.

Water model: A simple point charge-extended (SPC/E) model was used for water molecules, due to its excellent description for bulky water.

Simulation methods

Molecular dynamics simulations were performed using the NAMD 2.9 simulation package²⁸. VMD was used to visualize the system²⁹.

Each simulation box contained one separation device as shown in Figure 2, with 14,040 to 38,968 water molecules in each box depending on the model and the size of simulation box, with a water density of 1.0 g/cm³ in the bulk. The 12-6 Lennard-Jones (LJ) parameters for the carbon atoms are $\sigma = 0.382$ nm and $\epsilon = 0.086$ kcal/mol, and those for the oxygen atoms are $\sigma = 0.354$ nm and $\epsilon = 0.152$ kcal/mol, which are adopted from

Hummer's work². Ions (Na^+ and Cl^-) with specific salt concentrations were added and neutralized the system. All other parameters were adopted from CHARMM27 force-field. Particle mesh Ewald (PME) calculation was used for treatment of the electrostatic interaction. 5 ns NVT and NPT simulation were conducted respectively to fill the membrane with water molecules, along with the pre-equilibration of the whole system under 1 atm before the hydrostatic pressure was applied. The solvated area outside membrane was then ionized with NaCl of different concentrations. The water layer is around 20-25 Å in thickness at each side of the membrane, and the size of the unit cell depends on the CNT entrance and stage number (56 Å per stage in depth and 29 Å per entrance in wide). For example, the size of 4-entrance 3-stage HC-CNT simulation box is 42 Å×142 Å×210 Å.

Periodic boundary condition was applied in all directions. To prevent the membranes from being deformed, carbon atoms were fixed during all the simulations. All the systems underwent 1000-step energy minimization before the simulations. Langevin thermostat was incorporated to ensure the constant temperature (300 K), and Langevin pressure control was adopted during the NPT equilibration. Each simulation lasted 60-100 ns depending on the size of the simulation box. The first 5 ns was discarded and the rest were used to perform our analysis. A time step of 2 fs was used, and the data were collected every 1000 steps.

Hydrostatic pressure difference is incorporated via the method developed by Zhu *et al.*^{30,31} A constant force is applied on water molecules between the membranes, for example, $z < -100$ Å and $z > 100$ Å. This creates a pressurized driving force given by $\Delta P = nf / A$, where n is the number of water molecules to which the force is applied, and A is the cross section area of the membrane. In our simulations, both the numbers of water molecules and the constant force have been adjusted to ensure that a constant pressurized driving force is generated.

The potential of mean force (PMF) of a given ion at the Y-junction were performed using umbrella sampling derived from adaptive biasing force (ABF) simulations. One-dimensional harmonic biasing potential along the upper or lower branch CNT axis was exerted on the test ion. The harmonic force constant ranges from 0.1 to 1.0 kcal/(mol·Å²) for each simulation. For all the simulations, a window width of 0.1 Å was adopted, and the simulation duration of 5 ns was used. The extension of extra 2 ns simulation did not significantly alter the PMF profile.

Electric potential was calculated using the formula

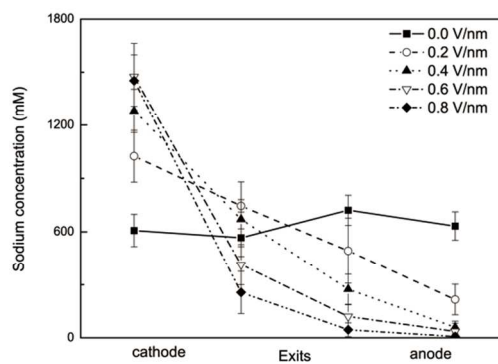
$$E(y) = \sum_{i \in (y-\Delta y, y+\Delta y)} \frac{q_i}{4\pi\epsilon_r}, \text{ where } E(y) \text{ is the electric potential at a specific position on the y-axis, and } i \text{ is the charged molecules at position approximately equal to } y \text{ (with an error of } \Delta y) \text{ in the box with } q_i \text{ being its charge, and } \epsilon_r \text{ is the dielectric constant in water.}$$

Results and Discussion

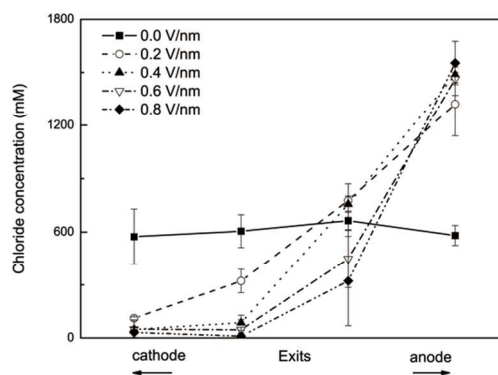
Simulation of the desalination process

The salt concentrations of the outlet streams from the HC-CNT membrane apparatus with four entrances, four outlets (with pore density $6.7 \times 10^{12}/\text{cm}^2$) and three stages of partitioning,

respectively, are given in Figure 3. NaCl concentration at entrance is set at 500 mM, which is close to the average salt concentration of seawater. The pressure applied on the molecules at entrance is 300 MPa and the electric field strength ranges from 0.0 to 0.8 V/nm.



(a)



(b)

Fig. 3 The ion translocation in 1.6-nm-diameter, 4-entrance, 3-stage HC-CNT (a) sodium (b) chloride concentration at four exits when exposed to different electric field strength. (a) Sodium concentrations at four exits under different electric field strength. (b) Chloride concentrations at four exits under different electric field strength.

The concentrations of Na^+ and Cl^- at the outlet of the chamber at different electric field strengths are given in Figure 3 (a) and Figure 3 (b), respectively. The increase in the electric field leads to a reduction of Na^+ concentration at anode outlets and meanwhile monotonic increase at the cathode outlets. The Cl^- concentrations of outlets response similarly to the increase of the electric field strength. All these lead to the generation of low ion concentration flux from the central outlets while concentrated ion flux from the outlets at the electrode area.

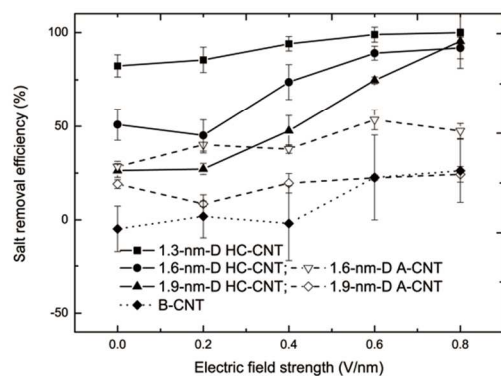


Fig. 4 Salt removal efficiency with regards to electric field strength at different CNT models

Figure 4 gives the salt removal efficiency (SRE) determined by following equation:

$$SRE = 1 - \frac{C_{out}}{C_{entr}}$$

in which C_{out} and C_{entr} are ion concentrations at the central outlets and entrances, respectively. Two crucial implications can be extracted: first of all, as expected from the ion translocation, ion removal performance of HC-CNT approaches nearly 100% when it comes to strong electric field. This indicates that the exertion of electric field offers a possible solution to increasing ion rejection without sacrificing the water flux. Secondly, both A-CNTs and B-CNTs fail to achieve the same outcome, with ion removal efficiency below 50% even if electric field as large as 0.8 V/nm is applied. This suggests that the unique structure of HC-CNT accounts for its effectiveness. The detailed explanations for the failure of other two models, however, are disparate, as detailed in the later portion of this work.

It might be surprising at first sight that SREs of HC-CNT and A-CNT are not zero when electric field is not applied. However, recall that the size exclusion effect of CNTs can expel ions effectively as well. Therefore, even if the electric field is absent, both two models exhibit certain ion rejection, which increases as CNT diameter decreases. This is consistent with the simulation result of Corry.^{5,9}

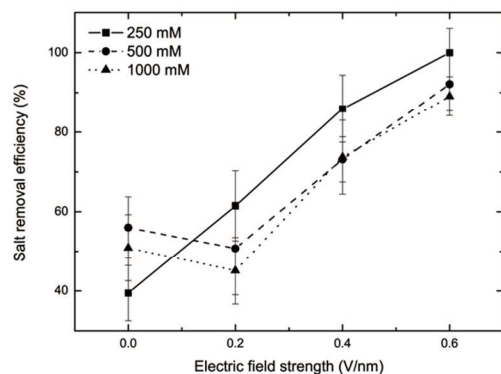


Fig. 5 Salt removal efficiency of HC-CNT under different ion concentration as the function of electric field strength

The effect of salt concentration on this electrokinetic desalination was examined. Considering that seawater salinity is between 400 mM and 600 mM, where the salt concentration of brackish water ranges from 10 to 500 mM, we choose 250 mM, 500 mM and 1000 mM as the input water salinities. The effect of salinity on desalination performance is shown in Figure 5, where no significant difference in salt removal ratio is observed, indicating that HC-CNT is applicable to both seawater and brackish water.

Separation mechanism

From figure 4, the lack of connectivity (A-CNT) is followed by the disappearance of ion preference on outlets, which provides a strong argument for the claim that the function of electric field is to provide the driving force for ion translocation. In other words, the lack of connectivity in A-CNT accounts for its inability to separate ions and water molecules.

To provide a more quantitative analysis, free energy changes for ions to move upward or downward at the Y-junction were calculated using PMF, and the free energy differences between two paths were derived and given in Figure 6.

It is shown in Figure 6 that the free energy barrier is larger than 2.0 kcal/mol for Na^+ and Cl^- to move to opposite direction of the electrical force. This value agrees with the work needed for the electrical force to move ions from the lower to the upper branch. Moreover, the free energy barrier boosts against the increase of electric field strength. These suggest that the effectiveness of ion translocation is determined by the free energy barrier at the Y-junction created from the external electric field.

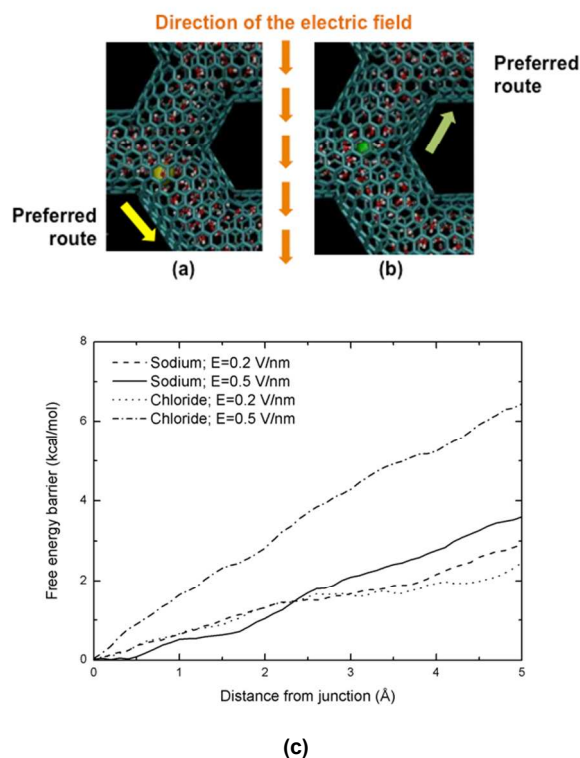


Fig. 6 Schematic illustration for Na^+ (a) and Cl^- (b) to move towards cathode and anode at the Y-junction; (c) free energy difference between two paths under different electric field strength

It is illustrated from above results the efficacy and mechanism of electrokinetic desalination using HC-CNT. However, there are two challenging questions that may reject the use of HC-CNT. Firstly, the energy consumption: why is electric field strength used in our simulations formidably large? Secondly, water flux: will electric field affect water flux across HC-CNT? It is also interesting to compare the transmembrane water flux of HC-CNT with existing membranes.

Energy consumption

The answer to the first question will be dissected into two sections. First of all, we will extrapolate our simulation results where the magnitude of electric field exceeds the reasonable range to the real cases where the electric field applied is mild and feasible. The major reason for applying such a high electric field lies in the spatial and temporal limitation of simulations, i.e., the separation must be completed in nanoseconds and within three stages (roughly 16.2 nm). This stands in great contrast to the real cases where the membrane thickness is at least of several centimetres and retention time of ions inside can be more than seconds.

If we assume that the electric field needed to achieve similar salt removal ratio is linearly decreasing with the thickness of the membrane and also the flow rate, we can have an electric field which is 10^9 - 10^{10} -fold smaller (10^7 - 10^8 from size expansion and 10^2 from the reduction of hydrostatic pressure difference). Overall, the ion retention time is greatly extended in the real cases, and eventually we can come up with an electric field whose strength is roughly around 0.1-1 V/m, which is equivalent to the voltage smaller than 1.0 V applied to the membrane. This estimation is sketchy, but it matches with the reasonable range of voltages (<1.2 V) currently exercised in CDI process²².

To justify the assumption that electric field needed for thicker membrane is smaller, we performed simulations regarding different stage numbers (Figure 7). Figure 7 (a) indicates that more stage number leads to weaker electric field in achieving similar desalination performance. This matches what is known in flow-field fractionation³² that the separation performance depends on the ratio of the retention time and driving force.

The other question regarding energy consumption is that whether using electrokinetic approach is cost-effective compared with typical desalination process like CDI and RO. It might be disappointing that methods to calculate energy consumption from simulations are seldom reported. Therefore, we will avoid the direct comparison between energy consumptions from simulations and experiments. Instead, we will compare data from two simulation models, HC-CNT and B-CNT, which represent our proposed desalination apparatus and CDI, respectively. A quick reminder from Figure 4 is that B-CNT will consume much more energy if similar salt removal ratio is obtained, which implies that our proposed apparatus is more likely to save energy. The explanation for this energy reduction is illustrated in Figure 8.

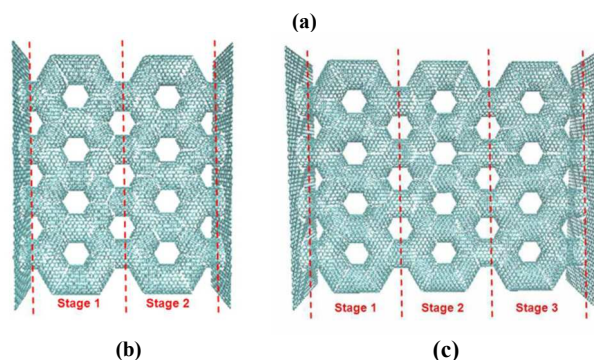
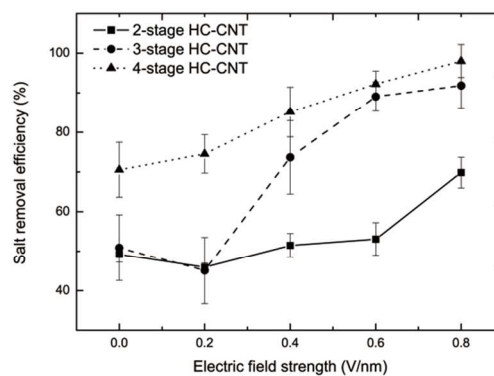


Fig. 7 (a) Salt removal ratio of two-stage and three-stage HC-CNT model as a function of electric field strength; (b)(c) Illustration of two-stage (b) and three-stage (c) HC-CNT.

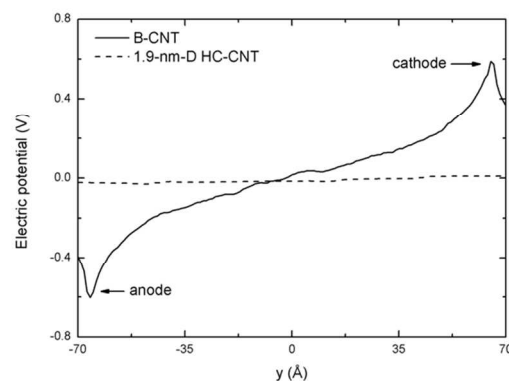


Fig. 8 Electric potential of B-CNT and HC-CNT at the outlets when exposed to $E=0.6$ V/nm.

In Figure 8, electric potential for B-CNT resembles what is implied in the Debye theory, where there will be a double-layer with an exponential decrease in electric potential when it comes to a typical CDI device³³⁻³⁵. In this case, the ion translocation at different sides creates an electric potential difference, which is opposite to and at the same order of magnitude of the electric field applied. This greatly reduces the energy effectiveness. In HC-CNT, however, confinement results in much less ions inside the membrane, and eventually small electric potential difference is observed.

Water flux

The remaining question is that whether the application of electric field affects the water flux. Figure 9 provides the water conductance, as well as the total water flux before and after the exercise of electric field.

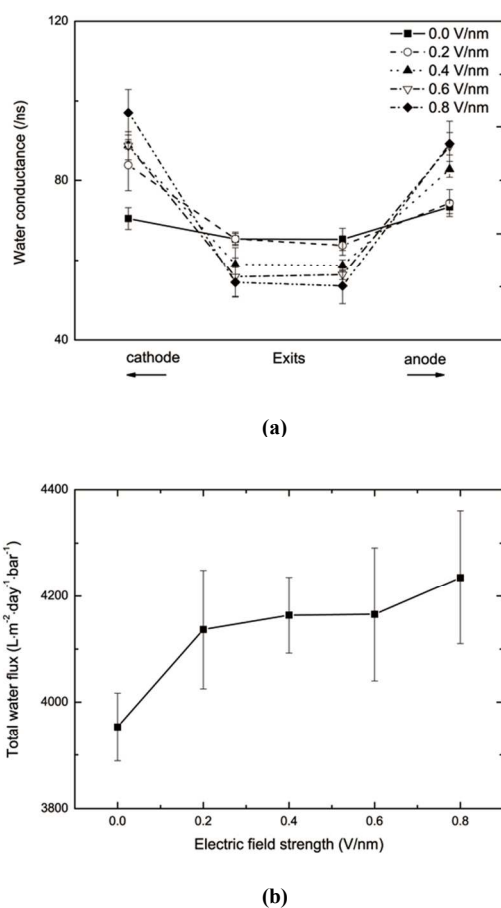


Fig. 9 (a) Water conductance at different exits in 1.6-nm-diameter, 4-entrance, 3-stage HC-CNT. (b) The total water flux extrapolated from simulation data as the function of electric field strength.

Despite that the water molecules tend to follow ions and translocate to cathode or anode outlets, the total water flux has even embraced a slight increase. The consistency between water and ion translocation is not a coincidence: it is probably due to the osmotic pressure difference caused by the ion translocation along the y-axis.

It is noteworthy that only the water leaving at the dilute region will be collected and counted as the “fresh water flux”. The ratio of fresh water flux over total water input flux is denoted as fresh water recovery. Typically in our simulations, the fresh water recovery is around 50%. However this value is not necessarily that limited in experiments. The fresh water recovery can be well expected to embrace an increase if we scale up the system by expanding the membrane area along the y-axis and the membrane thickness along the z-axis while keeping the electric field strength constant. Given that the same ratio of membrane thickness over membrane area guarantees that most ions will move towards the upmost or downmost outlets, we can increase the fresh water recovery ratio to 80% in case of 10 outlets or 90% for 20 outlets.

Now we come to examine the advantage of HC-CNT over other desalination membrane materials. The comparison between HC-CNT and other CNT membranes are labelled in Figure 10.

Figure 10 reiterates what is mentioned before: the long-standing problem of CNT as RO membrane material lies in the lack of mechanism to distinguish ions and water molecules. Despite some elegant pioneering simulation and experimental works that pointed out the steric hindrance or electrostatic repulsion as the driving forces^{5, 9, 13, 17, 18, 20, 21}, we can still observe the dramatic decreases in ion rejection when the CNT size exceeds some critical values. However, the idea of using HC-CNT, at least from simulation side, proposes a new way of solving this issue. As previously reflected in Figure 4, the ion removal ratio does not depend on the size of CNT, which allows for larger size CNT to be used for HC-CNT and eventually the faster water flux. This advantage makes the realization of HC-CNT more tempting: the higher water flux can compensate for the additional energy consumption, not to mention that CNT membranes already exhibit ultra-fast water transport property.

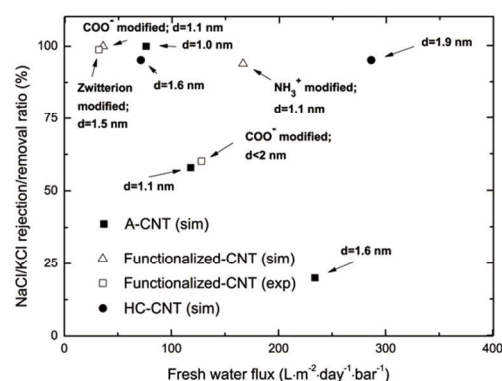


Fig. 10 Comparison between HC-CNT and other CNT membranes. A-CNT data are either from reference [5] or reproduced using similar simulations; Functionalized-CNT simulation data are from reference [9], while experimental data are extracted from reference [17, 18] and [20].

From Simulations to Experiments

Notably, the HC-CNT is not far from experimental practices. First of all, applying electric field is much easier than imposing electric charges on CNT surface. Secondly, CNT diameters in our simulation range from 1.3 nm to 1.9 nm, which does not go beyond the experimental availability: Holt et al.¹² and Kim et al.³⁶ have reported the fabrication of 1.6-nm-diameter and 1.2-nm-diameter carbon nanotubes respectively. Thirdly, pore density in our simulations is around $6.7 \times 10^{12} / \text{cm}^2$, which is within the scope of experimental studies³⁷⁻⁴⁰. Furthermore, a wide range of techniques have been developed to synthesize Y-shaped CNT, including chemical vapour deposition⁴¹⁻⁴³, alumina templates⁴⁴, growth via catalysts⁴⁵, and electron beam nano-welding⁴⁶. In addition to Y-shaped morphology, connectivity can also be obtained by packed CNTs, which have already been subjected to mass production⁴⁷. Lastly, the ion concentrations in our studies range from 250 mM to 1000 mM, and hydrostatic pressure applied is 300 MPa. Although these values are larger than expected, it allows more ion permeation events to reduce

uncertainty generated from statistical errors.

Despite what is discussed above, there are several points that remain to be clarified by experiments. First of all, the non-uniformity of the honeycomb structure might lead to the loss of separation efficiency; secondly, it is difficult to measure energy consumption accurately using the current methodology. Above all, the synthesis of HC-CNTs and the design of device are crucial to the realization of the idea.

Also, it has not escaped our notice that nanomaterials other than carbon nanotubes with honeycomb structure might be serving as good candidates for desalination. For example, there have been both simulation^{48, 49} and experimental reports⁴⁹ about metal-organic frameworks in various structures that might facilitate the desalination process.

Conclusions

We have shown that coupling external electric field with HC-CNT, a novel CNT topology structure, significantly enhances the desalination performance of CNT membrane. Over 95% salt rejection and around 50% fresh water recovery have been achieved in our simulations by using 0.8 V/nm electric field. The seemingly formidably large values are in fact within the scope of experimental practices with a reasonable combination of stage numbers and electric fields. Moreover, CNT diameter is critical to ion rejection performance without the electric field, but it makes not much difference for our module when a strong electric field is applied. This attribute enables HC-CNT to yield much higher water flux compared with the CNT RO membranes while a high ion rejection is maintained. In addition to its advantage over CNT RO membranes, the limited accessibility for ions and water molecules to confinement inside membranes reduces the electric potential difference after the ion translocation takes place, which might have greatly increase the economic feasibility of electrokinetic desalination process.

Likewise, ion concentration influences the desalination slightly, indicating the wide range of input water salinity that our model can be applied to, covering from brackish water to seawater.

The separation mechanism is subjected to the discussion here. The addition of the electric field allows ion translocation vertical to the flow direction. PMF profile reveals a free energy barrier as large as 2.0-6.0 kcal/mol for ions to move opposite to the direction of electrical force, which results in the spatial separation. Based on the mechanisms discussed above, we believe that this novel topology structure CNT sheds light on the complex CNT membrane design for desalination aside from traditional aligned CNTs.

Acknowledgement

The authors are grateful to the Chinese National Natural Science Foundation for financial support of this project (No. 21276138) and 973 Project (No.2013CB733604), as well as Tsinghua University Fundamental Project (No. 20131089301)

Note and reference

Department of Chemical Engineering, Tsinghua University, Beijing, 100084, China.

E-mail: ludianan@tsinghua.edu.cn; liuzheng@tsinghua.edu.cn

- M. A. Montgomery and M. Elimelech, *Environ Sci Technol*, 2007, 41, 17-24.

- G. Hummer, J. C. Rasaiah and J. P. Noworyta, *Nature*, 2001, 414, 188-190.
- S. Granick and S. C. Bae, *Science*, 2008, 322, 1477-1478.
- K. Falk, F. Sedlmeier, L. Joly, R. R. Netz and L. Bocquet, *Nano Lett*, 2010, 10, 4067-4073.
- B. Corry, *J Phys Chem B*, 2008, 112, 1427-1434.
- X. H. Sun, J. Wu, Z. Q. Chen, X. Su and B. J. Hinds, *Adv Funct Mater*, 2013, 23, 1500-1506.
- C. H. Ahn, Y. Baek, C. Lee, S. O. Kim, S. Kim, S. Lee, S. H. Kim, S. S. Bae, J. Park and J. Yoon, *J Ind Eng Chem*, 2012, 18, 1551-1559.
- M. G. Buonomenna, *Desalination*, 2013, 314, 73-88.
- B. Corry, *Energ Environ Sci*, 2011, 4, 751-759.
- M. F. L. De Volder, S. H. Tawfik, R. H. Baughman and A. J. Hart, *Science*, 2013, 339, 535-539.
- M. Majumder, N. Chopra, R. Andrews and B. J. Hinds, *Nature*, 2005, 438, 44-44.
- J. K. Holt, H. G. Park, Y. M. Wang, M. Stadermann, A. B. Artyukhin, C. P. Grigoropoulos, A. Noy and O. Bakajin, *Science*, 2006, 312, 1034-1037.
- C. Song and B. Corry, *J Phys Chem B*, 2009, 113, 7642-7649.
- M. A. Yu, H. H. Funke, J. L. Falconer and R. D. Noble, *J Am Chem Soc*, 2010, 132, 8285-8290.
- S. Bandow, S. Asaka, Y. Saito, A. M. Rao, L. Grigorian, E. Richter and P. C. Eklund, *Phys Rev Lett*, 1998, 80, 3779-3782.
- O. Jost, A. A. Gorbunov, W. Pompe, T. Pichler, R. Friedlein, M. Knupfer, M. Reibold, H. D. Bauer, L. Dunsch, M. S. Golden and J. Fink, *Appl Phys Lett*, 1999, 75, 2217-2219.
- M. Majumder, X. Zhan, R. Andrews and B. J. Hinds, *Langmuir*, 2007, 23, 8624-8631.
- B. J. Hinds, N. Chopra, T. Rantell, R. Andrews, V. Gavalas and L. G. Bachas, *Science*, 2004, 303, 62-65.
- Q. W. Chen, L. Y. Meng, Q. K. Li, D. Wang, W. Guo, Z. G. Shuai and L. Jiang, *Small*, 2011, 7, 2225-2231.
- F. Fornasiero, H. G. Park, J. K. Holt, M. Stadermann, C. P. Grigoropoulos, A. Noy and O. Bakajin, *P Natl Acad Sci USA*, 2008, 105, 17250-17255.
- W. F. Chan, H. Y. Chen, A. Surapathi, M. G. Taylor, X. H. Hao, E. Marand and J. K. Johnson, *ACS Nano*, 2013, 7, 5308-5319.
- Y. Oren, *Desalination*, 2008, 228, 10-29.
- X. J. Gong, J. C. Li, C. Guo, K. Xu and H. Yang, *Nanotechnology*, 2013, 24.
- T. A. Beu, *J Chem Phys*, 2011, 135.
- M. Mouri, M. Ogawa and S. Souma, *J Appl Phys*, 2012, 112.
- J. Y. Su and H. X. Guo, *ACS Nano*, 2011, 5, 351-359.
- <http://www.ks.uiuc.edu/Research/vmd/plugins/nanotube/>.
- L. Kale, R. Skeel, M. Bhandarkar, R. Brunner, A. Gursoy, N. Krawetz, J. Phillips, A. Shinozaki, K. Varadarajan and K. Schulten, *J Comput Phys*, 1999, 151, 283-312.
- W. Humphrey, A. Dalke and K. Schulten, *J Mol Graph Model*, 1996, 14, 33-38.
- F. Q. Zhu, E. Tajkhorshid and K. Schulten, *Biophys J*, 2002, 83, 154-160.
- F. Q. Zhu, E. Tajkhorshid and K. Schulten, *Biophys J*, 2004, 86, 256A-256A.
- J. C. Giddings, *Science*, 1993, 260, 1456-1465.
- P. M. Biesheuvel and A. van der Wal, *J Membrane Sci*, 2010, 346, 256-262.
- P. M. Biesheuvel, B. van Limpt and A. van der Wal, *J Phys Chem C*, 2009, 113, 5636-5640.
- R. Zhao, P. M. Biesheuvel, H. Miedema, H. Bruning and A. van der Wal, *J Phys Chem Lett*, 2010, 1, 205-210.
- S. Kim, J. R. Jinschek, H. Chen, D. S. Sholl and E. Marand, *Nano Lett*, 2007, 7, 2806-2811.
- G. F. Zhong, J. H. Warner, M. Fouquet, A. W. Robertson, B. A. Chen and J. Robertson, *ACS Nano*, 2012, 6, 2893-2903.
- M. Yu, H. H. Funke, J. L. Falconer and R. D. Noble, *Nano Lett*, 2009, 9, 225-229.
- D. N. Futaba, K. Hata, T. Yamada, T. Hiraoka, Y. Hayamizu, Y. Kakudate, O. Tanaike, H. Hatori, M. Yumura and S. Iijima, *Nat Mater*, 2006, 5, 987-994.

-
40. S. Esconjauregui, M. Fouquet, B. C. Bayer, C. Ducati, R. Smajda, S. Hofmann and J. Robertson, *Acs Nano*, 2010, 4, 7431-7436.
41. B. C. Satishkumar, P. J. Thomas, A. Govindaraj and C. N. R. Rao, *Appl Phys Lett*, 2000, 77, 2530-2532.
- 5 42. W. Z. Li, J. G. Wen and Z. F. Ren, *Appl Phys Lett*, 2001, 79, 1879-1881.
43. F. L. Deepak, A. Govindaraj and C. N. R. Rao, *Chem Phys Lett*, 2001, 345, 5-10.
- 10 44. C. Papadopoulos, A. Rakitin, J. Li, A. S. Vedenev and J. M. Xu, *Phys Rev Lett*, 2000, 85, 3476-3479.
45. N. Gothard, C. Daraio, J. Gaillard, R. Zidan, S. Jin and A. M. Rao, *Nano Lett*, 2004, 4, 213-217.
46. M. Terrones, F. Banhart, N. Grobert, J. C. Charlier, H. Terrones and P. M. Ajayan, *Phys Rev Lett*, 2002, 89, 89.
- 15 47. Q. Zhang, J. Q. Huang, M. Q. Zhao, W. Z. Qian and F. Wei, *Chemsuschem*, 2011, 4, 864-889.
48. Z. Q. Hu, Y. F. Chen and J. W. Jiang, *J Chem Phys*, 2011, 134, 134.
- 20 49. J. W. Jiang, *Mol Simulat*, 2014, 40, 516-536.